A. Elola, E. Aramendi, U. Irusta, P. O. Berve and L. Wik, "*Multimodal Algorithms for the Classification of Circulation States During Out-of-Hospital Cardiac Arrest,*" in **IEEE Transactions on Biomedical Engineering**, vol. 68, no. 6, pp. 1913-1922, June 2021, doi: 10.1109/TBME.2020.3030216

Multimodal algorithms for the classification of circulation states during out-of-hospital cardiac arrest

Andoni Elola, Elisabete Aramendi*, *Member IEEE*, Unai Irusta, *Member IEEE*, Per Olav Berve, Lars Wik

Abstract*—*Goal: **Identifying the circulation state during out-of-hospital cardiac arrest (OHCA) is essential to determine what life-saving therapies to apply. Currently algorithms discriminate circulation (pulsed rhythms, PR) from no circulation (pulseless electrical activity, PEA), but PEA can be classified into true (TPEA) and pseudo (PPEA) depending on cardiac contractility. This study introduces multi-class algorithms to automatically determine circulation states during OHCA using the signals available in defibrillators.** ***Methods:*** **A cohort of 60 OHCA cases were used to extract a dataset of 2506 5-s segments, labeled as PR (1463), PPEA (364) and TPEA (679) using the invasive blood pressure, experimentally recorded through a radial/femoral cannulation. A multimodal algorithm using features obtained from the electrocardiogram, the thoracic impedance and the capnogram was designed. A random forest model was trained to discriminate three (TPEA/PPEA/PR) and two (PEA/PR) circulation states. The models were evaluated using repeated patient-wise 5-fold cross-validation, with the unweighted mean of sensitivities (UMS) and F_1-score as performance metrics.** ***Results:*** **The best model for 3-class had a median (interquartile range, IQR) UMS and F_1 of 69.0% (68.0-70.1) and 61.7% (61.0-62.5), respectively. The best two class classifier had median (IQR) UMS and F_1 of 83.9% (82.9-84.5) and 76.2% (75.0-76.9), outperforming all previous proposals in over 3-points in UMS.** ***Conclusions:*** **The first multiclass OHCA circulation state classifier was demonstrated. The method improved previous algorithms for binary pulse/no-pulse decisions.** ***Significance:*** **Automatic multiclass circulation state classification during OHCA could contribute to improve cardiac arrest therapy and improve survival rates.**

***Index Terms*—Random Forest, Machine Learning, Cardiac arrest, pulsed rhythm (PR), pulseless electrical activity (PEA), pseudo pulseless electrical activity.**

I. INTRODUCTION

OUT of hospital cardiac arrest (OHCA) is a major public health problem in the industrialized world, with an annual incidence of 41 (range 19-104) cases treated per 100 000 persons in Europe [1], and more than 350 000 cases reported annually by the resuscitation outcome consortium in the USA [2]. Despite recent advances in treatment and monitoring, survival rates with good functional status remain around 9% in adults [2]. Cardiac arrest can happen without warning. The patient abruptly loses the respiratory and cardiovascular functions, leading to unconciousness and ultimately death if the patient is not treated within a few minutes. The chain of survival metaphor specifies the key steps to improve OHCA survival rates. Those steps are: early recognition of the arrest, early treatment including cardiopulmonary resuscitation (CPR) and defibrillation, and post-resuscitation care. CPR includes effective chest compressions and ventilations, coordinated with defibrillation therapy provided with either basic automated external defibrillators (AED) or advanced monitor/defibrillators. Specialized interventions may include advanced monitoring, pharmacological treatment, and if spontaneous circulation is restored, transport to a hospital for post-resuscitation care [3], [4].

The objective of resuscitation therapies is to restore spontaneous circulation (ROSC) or pulse, i.e. the cardiac function of the patient. However, during therapy OHCA patients undergo frequent and dynamic rhythm transitions [5]. It is therefore key to recognize and monitor the patient's response to treatment, particularly the identification of spontaneous pulse. Rapid recognition of ROSC would avoid unnecessary chest compressions that could lead the patient into VF again [6], and would anticipate the benefit of post-resuscitation treatment [7]. More specifically, algorithms or methods are needed to discriminate pulseless electrical activity (PEA) from pulse generating rhythms (PR) [8], [9]. During PEA, patients present a (quasi)-normal electrocardiogram with discernible heartbeat activity (QRS complexes), but no associated mechanical contractions. A state known as electromechanical dissociation.

Pulse detection in OHCA patients is challenging. Palpation techniques have a low specificity (55%) and require long interruptions ($>$ 10 s) in therapy [10]–[12]. Automated pulse identification using the electrocardiogram (ECG) is challenging because PEA and PR rhythms show an organized ECG with discernible QRS complexes [13]. Chest conductivity is affected by transport of oxygenated blood, so the thoracic impedance (TI) signal is also of value to identify pulse during OHCA [8]. In the last decade, various algorithms have been proposed for PEA/PR discrimination during OHCA using only the ECG [13], [14], the thoracic impedance [15],

Manuscript submitted X, 2020; accepted X, X. This work was supported by the Spanish Ministerio de Ciencia, Innovación y Universidades through grant RTI2018-101475-BI00, jointly with the Fondo Europeo de Desarrollo Regional (FEDER), and by the Basque Government through grants IT1229-19 and PRE_2019_2_0100

Asterisk indicates corresponding author.

*E. Aramendi is with the Department of Communications Engineering, University of the Basque Country UPV/EHU, Ingeniero Torres Quevedo Plaza, 1, 48013, Bilbao, Spain (e-mail: elisabete.aramendi@ehu.eus).

A. Elola and U. Irusta are with the Department of Communications Engineering, University of the Basque Country UPV/EHU, Ingeniero Torres Quevedo Plaza, 1, 48013, Bilbao, Spain.

Per Olav Berve and Lars Wik are with the Norwegian National Advisory Unit on Prehospital Emergency Medicine (NAKOS), Norway.

[16] or a combination of both signals [8], [9], [17]. More recently, physiological signals affected by cardiac output like capnography or photoplethysmography have been incorporated to PEA/PR discrimination algorithms [18], [19].

One key limitation of all these contributions is to define a binary circulation state (pulse/no-pulse). PEA can be further classified into true-PEA (TPEA) and pseudo-PEA (PPEA) [20]. During PPEA echocardiography studies show that the electrical activity of the heart produces mechanical contractions, although of insufficient strength to maintain consciousness and adequate organ perfusion [21]. The two states of PEA have very different prognosis and treatment [22]–[24], and since PEA is the initial rhythm in up to 60% of OHCA cases [25], discriminating PPEA from TPEA is of great clinical interest. Echocardiography and invasive blood pressure (IBP) are the key technologies to discriminate PEA states, but they are rarely available during OHCA. Other methods based on ECG variables and end-tidal-CO2 ($EtCO_2$) values have also been proposed, but with inconclusive results [24], [26]–[28]. There is a need for automated circulation state classification algorithms that differentiate TPEA, PPEA and PR rhythms.

This study introduces a new multi-modal solution to classify circulation states during OHCA using concurrent information derived from the ECG, the TI and the capnogram. The solution allows the classification into two classes (PR/PEA) or three classes (TPEA/PPEA/PR), with the final aim of monitoring the circulation state of the patient and the response to resuscitation treatment. The study is based on an unique dataset that includes IBP signals measured using arterial lines during OHCA to provide an accurate ground truth clinical annotation of the circulation state.

II. Data collection and preprocessing

A. Dataset

The source of the data was a randomized OHCA clinical trial (No. NCT02479152), that investigated the hemodynamics of patients in cardiac arrest treated with manual cardiopulmonary resuscitation and mechanical chest compression devices. Data were recorded between 2015 and 2017 by the doctor manned car, part of the Air ambulance department of the Oslo Emergency Medical System (EMS) under the supervision of the principal investigator of the trial (coauthor Dr L. Wik). A total of 210 patients were included, from whom four signals were concurrently recorded using the Lifepak 15 (Stryker Ltd.) monitor-defibrillator: the ECG and the TI (recorded through the defibrillation pads), the sidestream capnogram, and the IBP signal acquired via onsite radial/femoral cannulation. In 135 cases cerebral oxygen saturation was continuously monitored in the right and left frontal lobes using the ForeSight Elite monitor (Casmed, Inc).

All signals were first converted to a common sampling rate of $f_s = 250\,\mathrm{Hz}$, and the capnogram was time-aligned with the ECG and the TI. Then signal intervals with the following characteristics were extracted: minimum duration 5-s, ECG in an organized rhythm (QRS complexes), and free of chest compression artefacts.

The ECG, TI and capnogram were used to develop the algorithms. A clinician and two expert biomedical engineers used all other sources of information to annotate the circulation state (TPEA, PPEA, PR) for each interval, including: clinical patient charts with annotated ROSC intervals, the IBP waveform, and cerebral oxygen saturation when available. Systolic (Sys), diastolic (Dias) and pulse pressure ($\mathrm{PP} = \mathrm{Sys} - \mathrm{Dias}$) were computed for each cardiac cycle and averaged to be displayed during annotation. The distinction between the three circulation states was possible using the objective values obtained from the IBP because systolic and pulse pressures are higher for PR than for PEA, and within PEA higher values are observed for PPEA than for TPEA. Fig. 1 shows a 150-s period with the signals recorded by the LifePak monitor, in which two intervals without chest compressions (as seen in the impedance) were extracted: a short 10-s PPEA interval (orange) around 15:39:00 with Sys/Dias/PP values of 54/34/20 mmHg, and a longer 40-s PR interval (green) around 15:40:40 with Sys/Dias/PP values of 147/67/80 mmHg.

A total of 300 intervals were identified from the 60 patients that had an IBP waveform. A median (interquartile range, IQR) of 5 (3-7) intervals was extracted per patient, with a median (IQR) duration of 27.6 (11.2-76.0) s. They were labeled as TPEA (129, from 37 patients), PPEA (75, from 26 patients) and PR (96, from 31 patients). The median (IQR) blood pressure values for the three circulation states in the extracted intervals are summarized in Table I. When the distributions were compared using a Mann-Whitney U test the systolic pressure and pulse pressure values were significantly higher for PR than for PPEA ($p < 0.001$), and for PPEA than for TPEA ($p < 0.001$).

TABLE I
Systolic (Sys), diastolic (Dias) and pulse pressure (PP) values for the three groups considered in this study

	TPEA	PPEA	PR
Sys (mmHg)	32.5 (24.6-41.7)	40.4 (35.0-49.1)	95.5 (68.9-148.7)
Dias (mmHg)	27.2 (19.5-36.4)	28.1 (25.9-33.7)	51.1 (40.0-75.9)
PP (mmHg)	4.1 (0.0-6.8)	11.3 (8.0-16.4)	45.4 (29.4-68.1)

The intervals were further divided into non overlapping 5-s segments. These segments were separated by 1-s in TPEA and PPEA for which the signals and the circulatory state of the patient are very variable. The PR segments were separated by 15-s because once a patient recovers pulse the circulatory state is more stable. As reference, the median duration of the PR and PEA intervals were 129-s and 15-s, respectively. These segments were used to design and validate the three (TPEA/PPEA/PR) and two (PEA/PR) circulation state classifiers. A total of 2506 5-s segments were obtained, for a median (IQR) of 42 (16-62) segments per patient, whereof 679 were TPEA, 364 PPEA and 1463 PR. Fig. 2 shows one example for each class. In the PPEA and PR segments there is a visible correlation between the ECG, the IBP and the impedance circulation component (ICC) (see Section III-B). For the TPEA the IBP is nearly flat, and there is no circulation component in the impedance. In addition the $EtCO_2$ values are displayed in the figure; these values were computed by averaging the $EtCO_2$ values of the ventilations in the previous minute [19].

III. Signal preprocessing

The ECG and TI were preprocessed to denoise the signals and extract components of interest. Multiresolution analysis

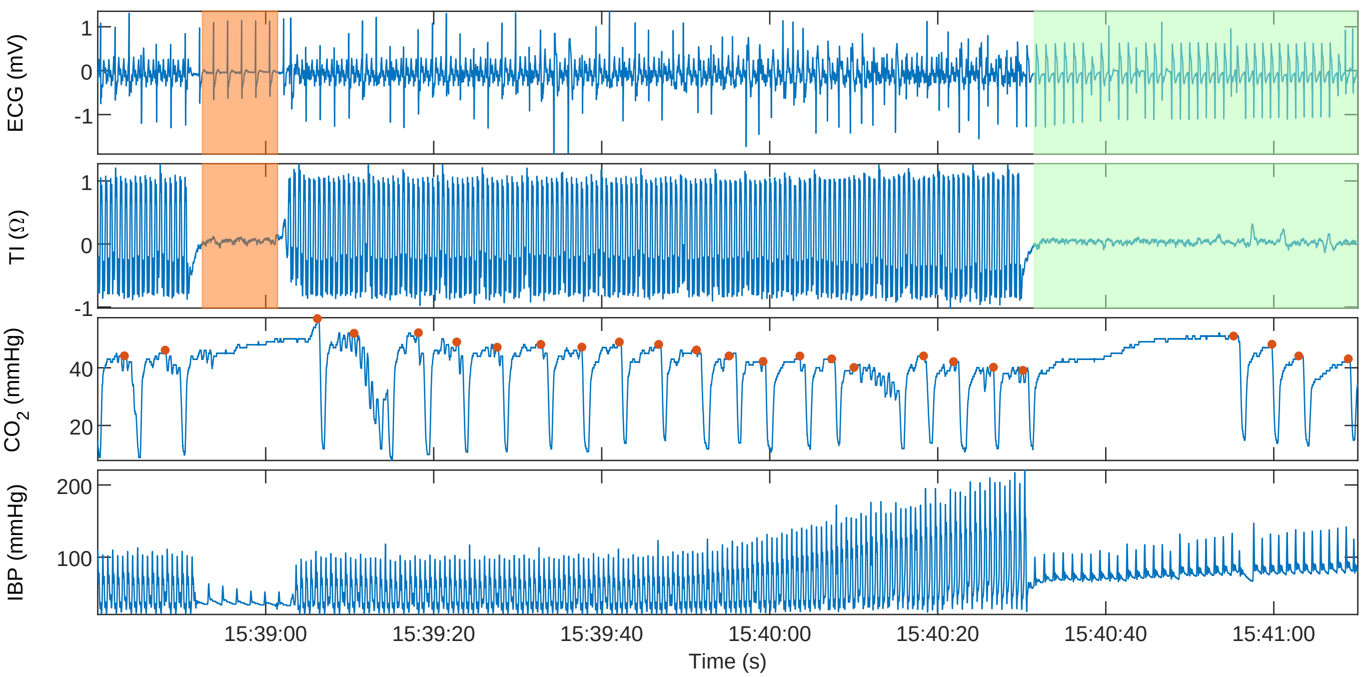

Fig. 1. A period of 150 s from a patient in OHCA is shown, where the ECG, the thoracic impedance (TI), and the capnogram can be observed together with IBP waveform, i.e. the signal used to annotate the pulse states. Two intervals are marked, a PPEA (in red) around 15:39:00 and a PR (in green) around 15:40:40. In the capnogram the $EtCO_2$ values computed for each ventilation are marked as dots (in red).

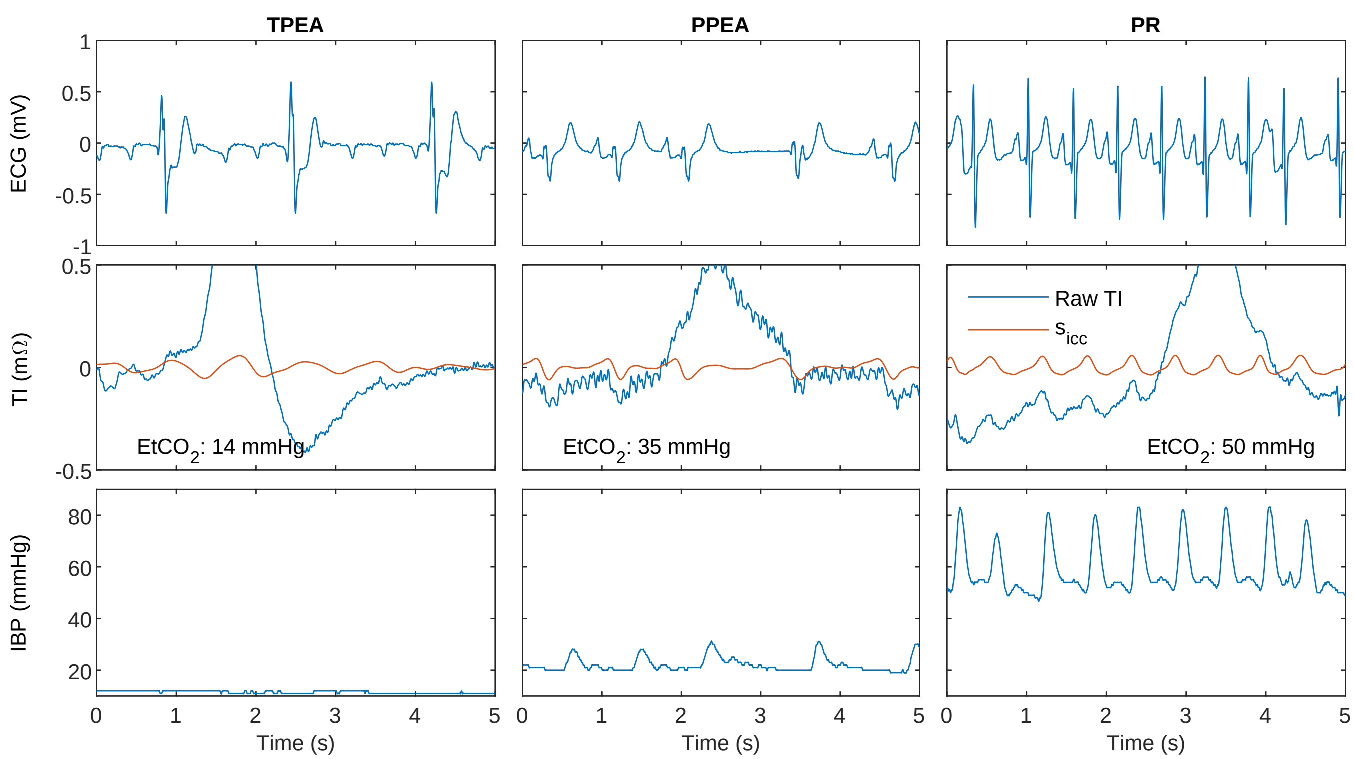

Fig. 2. Examples of segments annotated as true PEA (TPEA), pseudo PEA (PPEA) and PR. The ECG, the TI and the extracted circulation component (s_{icc}) are used by the algorithm together with the average $EtCO_2$ associated to each segment. The invasive blood pressure (IBP) permitted the labeling of the segments in the three classes.

based on stationary wavelet transform (SWT) was used to obtain the sub-band components or detail coefficients, and to denoise the signals using soft thresholding [29]. A Daubechies 4 mother wavelet was adopted [30].

A. The ECG

The ECG was decomposed in 8 levels of detail coefficients ($d_{1,\text{ecg}}$-$d_{8,\text{ecg}}$) and the threshold was estimated using $d_{2,\text{ecg}}$ to denoise $d_{3,\text{ecg}}$-$d_{8,\text{ecg}}$. A denoised ECG (s_{ecg}) was reconstructed using the denoised $d_{3,\text{ecg}}$ to $d_{8,\text{ecg}}$, which is equivalent to using the $0.5-31.25\,\text{Hz}$ bandwidth, adequate for the detection of pulse [13]. Fig. 3 shows the raw ECG, the denoised detail components $d_{3,\text{ecg}}$-$d_{7,\text{ecg}}$ and s_{ecg} for a PR case.

B. TI denoising and ICC extraction

The TI signal was first band-pass filtered in the 0.8-10 Hz band to remove baseline fluctuations and high frequency noise [8], [9], and then the ICC was obtained. The ICC shows the changes in TI produced by blood flow, and is associated to mechanical ventricular contractions [31]. The ICC can be modeled as a Fourier series, with a time changing fundamental frequency equal to the instantaneous heart rate [9], [32]. For a sampling period T_s and the discretized time axis $t_j = j \cdot T_s$, the ICC component at time t_j is expressed as [9]:

$$s_{\text{icc}}(t_j) = \sum_{k=1}^{K} a_k(t_j)\cos(2\pi k f(t_j)\cdot t_j) + b_k(t_j)\sin(2\pi k f(t_j)\cdot t_j) \tag{1}$$

where $f(t_j)$ is the beat-to-beat heart rate in Hz, and $a_k(t_j)$ and $b_k(t_j)$ are time-varying Fourier coefficients that will be estimated using Kalman filtering and smoothing, and the model uses K harmonics. The Kalman state vector $\boldsymbol{x}_j$ and the observation vector $\mathbf{H}_j$ are then:

$$\boldsymbol{x}_j = [a_1(t_j), \ldots, a_K(t_j), b_1(t_j), \ldots, b_K(t_j)]^T \tag{2}$$

$$\begin{aligned}\mathbf{H}_j = [&\cos(2\pi f(t_j)t_j), \ldots, \cos(2\pi f(t_j)Kt_j),\\ &\sin(2\pi f(t_j)t_j), \ldots, \sin(2\pi f(t_j)Kt_j)]\end{aligned} \tag{3}$$

In this work we assume a_k and b_k are gaussian processes [33], that can be updated as:

$$a_k(t_j) = \psi_j a_k(t_{j-1}) + w_j \tag{4}$$

$$b_k(t_j) = \psi_j b_k(t_{j-1}) + w_j \tag{5}$$

where w_j is a gaussian process with zero mean and standard deviation σ, and $\psi_j = \exp(-\lambda(t_j - t_{j-1}))$. The dynamic model can be expressed as:

$$\boldsymbol{x}_j = \boldsymbol{\Psi}_j \boldsymbol{x}_{j-1} + \mathbf{Q}_j \tag{6}$$

where $\boldsymbol{\Psi}_j = \psi_j \cdot \mathbf{I}_{2K}$, $\mathbf{Q}_j = \sigma \cdot \mathbf{I}_{2K}$ and $\mathbf{I}_{2K}$ is the identity matrix of order $2K \times 2K$.

The a_k and b_k coefficients were estimated using Rauch-Tung-Striebel smoother, as described in [33], [34], and $K = 5$ harmonics, $\lambda = 0.05$ and $\sigma = 0.01$ were used. The instantaneous heart rate, $f(t_j)$, was measured by detecting the R peaks in the ECG signal using the Hamilton-Tompkins algorithm [35].

The circulation component was reconstructed using $d_{5,\text{icc}} - d_{7,\text{icc}}$ ($\approx 1-8\,\text{Hz}$). Fig. 3 shows the s_{icc} and detail coefficients

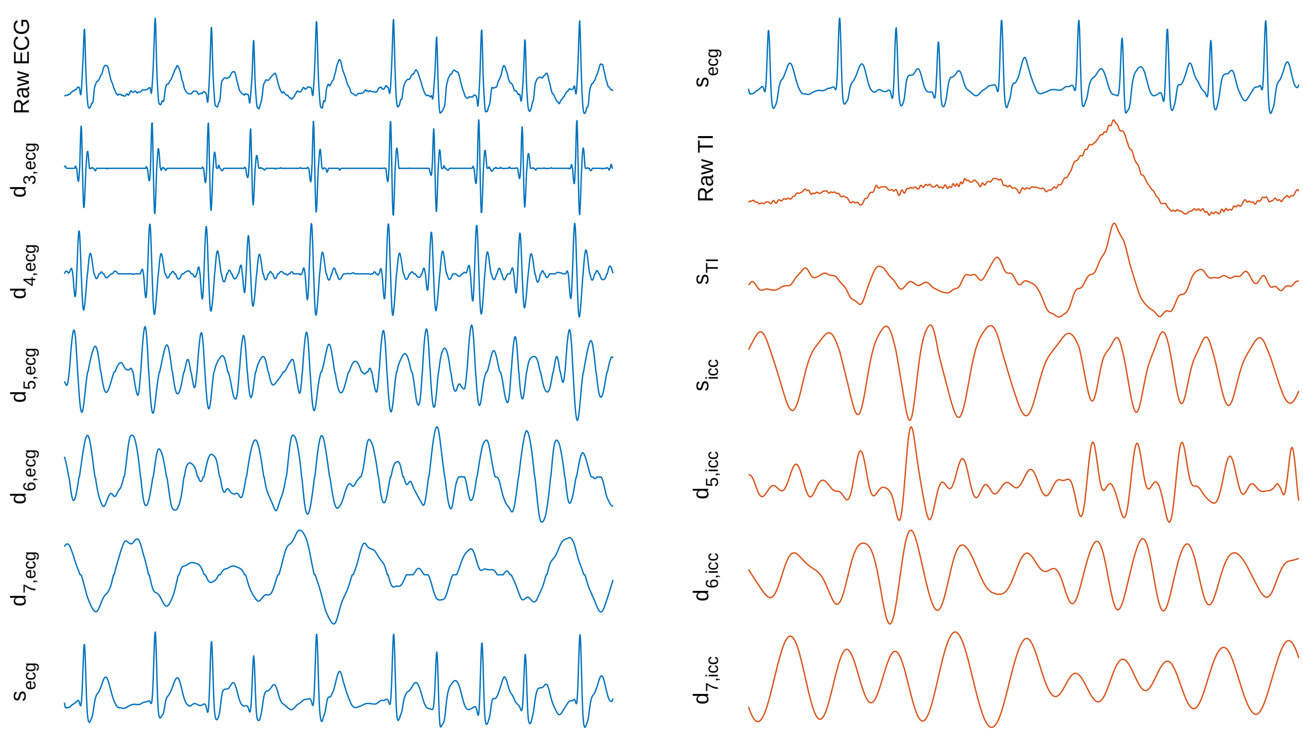

Fig. 3. Decomposition of the ECG and the TI signal into detail components using the stationary wavelet transform. The denoised ECG (s_{ecg}) and TI (s_{TI}) and the impedance circulation component (s_{icc}) are also shown.

for a PR case. As shown in the figure, the Kalman smoother is capable of obtaining the circulation component even in the presence of low frequency TI variations caused by ventilation, as observed in the band-passed impedance signal, s_{TI}.

C. *The capnogram*

$\mathrm{EtCO_2}$ values were automatically computed in the capnogram using the algorithm described in Aramendi et al. [36]. For each ventilation the $\mathrm{EtCO_2}$ value was marked as the maximum value of the capnogram in the expiration plateau, as shown by red dots in Fig. 1.

IV. Feature Engineering and Classification

A pletora of features, both described in the literature for PEA/PR discrimination, and new features proposed in this study for the same task were implemented.

A. *State of the art features*

A set of 37 features described in [8], [9], [13], [15], [17], [19], [32] were computed using the ECG, TI, ICC and capnography signals:

- **ECG:** Mean RR interval (`MeanRR`), variance of RR intervals (`VarRR`), mean and standard deviation of QRS peak-to-peak amplitudes (`MeanPP` and `StdPP`), median signal length (`MedianSL`), mean and variance of QRS width, QRS amplitude to duration ratio (`SlopeQRS`), median and variance of the signal after normalizing between 0 and 1 (`MSnorm` and `StdSnorm`), mean value of the signal, mean and standard deviation of the absolute value of the first difference of the signal (`MeanAbs1` and `StdAbs1`), the kurtosis of the averaged slope (`KurtSlp2`), amplitude spectrum area (`AMSA`), energy above 17.5 Hz (`HfP`) and Fuzzy entropy (`FuzzEn`).
- **TI:** Variance and cross-power (`XPwr`) as described in [17], peak of the power spectrum of the first difference of the signal in $1.5\,\mathrm{Hz} < f < 4.5\,\mathrm{Hz}$ range (`PkF`), and 10 features from the ensemble averaged signal as described in [8].
- **ICC:** Area per sample and mean area of s_{icc} and its first difference, Δs_{icc}. Mean and standard deviation of the peak-to-peak fluctuations of every beat in s_{icc} (`MeanPP` and `StdPP`), and the mean of Δs_{icc} (`MeanPP1`) [9], [32].
- **Capnogram:** The median value of the $\mathrm{EtCO_2}$ measured in the previous minute, $\mathrm{MEtCO_2}$, as described in [19].

B. *Novel features*

Pulsatility is associated to ECGs with narrower QRS complexes of larger amplitudes, and to waveforms in the ICC correlated to the heartbeats (QRS complexes). These differences should produce different characteristic waveforms in the detail coefficients for TPEA, PPEA and PR. The following features were extracted from s_{ecg}, $d_{3,\mathrm{ecg}} - d_{7,\mathrm{ecg}}$, s_{icc} and $d_{5,\mathrm{icc}} - d_{7,\mathrm{icc}}$ [37]–[39].

- Interquartile range (`IQR`).
- Sample entropy (`SampEn`) with an embedding dimension of 2 and tolerance of 0.2.
- Mean and standard deviation of the absolute value after normalizing to unit variance (`NMeanAbs` and `NMeanSd`).
- Mean and standard deviation of the absolute value of the first difference after normalizing to unit variance (`NMeanAbs1` and `NMeanSd1`).
- Skewness (`Skew`) and kurtosis (`Kurt`).
- Hjorth mobility (`Hmb`) and complextity (`Hcmp`).
- Phase-space representation was computed using Taken's time-delay embedding method with $\tau = 2$ and the skewness of pairwise distances was calculated (`SkewPS`).

Two extra features were computed for s_{ecg} and s_{icc}:

- The error of estimating the spectral power of the signal with a 4th order autorregresive Burg model (`ARErr`), best fit to signals with spectra concentrated around a fundamental frequency and its harmonics.
- The smoothed nonlinear energy operator (`SNEO`) as described in [40], which shows higher values for signals with higher amplitudes.

C. *Feature selection and classification*

The Random Forest (RF) classifier was adopted for both feature selection and classification. A RF is an ensemble of B decision trees that produce uncorrelated predictions, and uses a majority vote of the trees to produce the final label. Each tree was trained using the bootstrapping method with replacement and 50% of the data. The minority classes were over-sampled to have equal number of observations per class when training each tree and address class imbalance.

Data were partitioned patient-wise in a quasi stratified way into 5-fold cross validation partitions, and the procedure was repeated 100 times to statistically characterize the performance of the classifiers. In the training phase two RF classifiers were trained. The first RF classifier was trained using only the ECG and TI features, and was used for feature selection using permutation feature importance. At this stage minority classes were not over-sampled. The second RF classifier (final model) was trained using the most important N_f features and $\mathrm{MEtCO_2}$, and now the minority classes were over-sampled. Note that the total number of features in the final model was $N_f + 1$ when the $\mathrm{MEtCO_2}$ was considered.

D. *Model evaluation*

The models were evaluated using the per class sensitivity (Se) and $\mathrm{F_1}$-score. The unweighted mean of sensitivities (UMS) and the mean of the per class $\mathrm{F_1}$-scores ($\mathrm{F_{1m}}$) were used as global performance metrics. For the 2-class problem the area under the receiver operating characteristic curve (AUC) was also computed. The number of segments varied across patients, so all metrics were computed weighting each patient equally.

A multimodal model was evaluated integrating the three signals, ECG, TI and capnogram. Simple defibrillators and AEDs do not include a capnography module, so models based on the ECG and TI only were also developed. Finally, some lower cost AEDs do not record the TI with sufficient amplitude resolution to obtain the ICC [9], [13], so models using only the ECG were also developed.

V. RESULTS

A. Detailed classification of circulation states

The performance metrics for the detailed circulation state classifier are shown in Fig. 4 for models with an increasing number of features. The results in terms of UMS improved by less than 0.3-percent points for the models with more than $N_f = 30$ features, which had a median (IQR) F_{1m} and UMS of 61.5% (60.8-62.4) and 68.8% (67.7-69.8), respectively. The confusion matrix in Fig. 5 shows the detailed classification per group for the model with $N_f = 30$ features. The intermediate circulation state (PPEA) was the hardest to classify, since it may present PR or TPEA like characteristics depending on the degree of cardiac contraction.

The novel ICC feature extraction provided relevant information to classify circulation states. Fig. 6 shows the average feature ranking for all training partitions for a model with $N_f = 30$ features. The ranking was obtained as the probability of being included in the model after feature selection. As shown in the figure, our model for 30 features included 7 ICC features, but 3 of those were the ones with the highest probability to be included in the model. Some of the features were already proposed in the state of the art for PEA/PR classification, but other important features were first used in this study for circulation state classification. Note that $MEtCO_2$ was not included in the feature selection process and was added manually, so it is not present in Fig. 6.

The detailed (three-class) classification results depending on the available information (source signals) is shown in Table II. The TPEA and PPEA classes were most affected by constrained signal models, removing $MEtCO_2$ information decreased the F_1-score for TPEA by 3 points and for PPEA by 2 points. Further removing the TI produced a decrease in F_1-score of over 12 points for TPEA and 8 points for

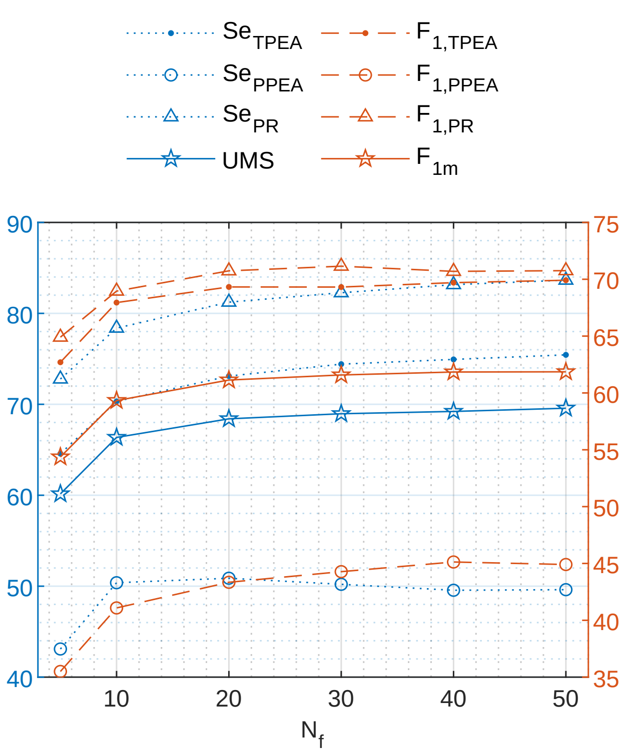

Fig. 4. Performance (%) of the prediction model in terms of the number of features included (N_f) for the three-class classification problem.

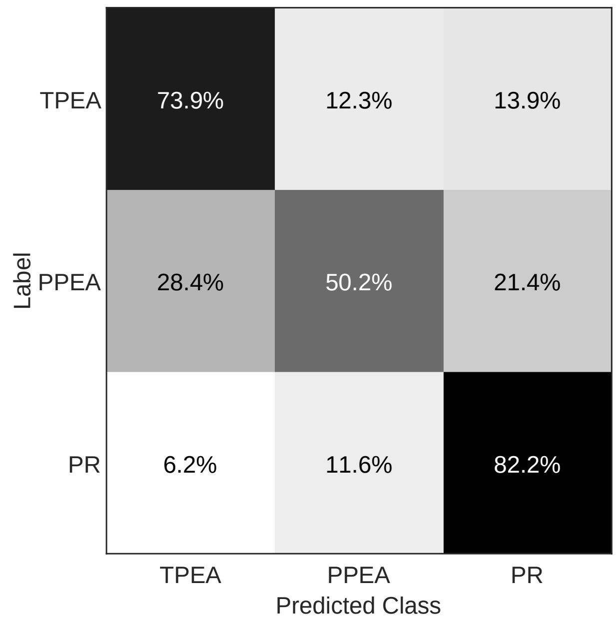

Fig. 5. Confusion matrix of the three-class circulation state classifier.

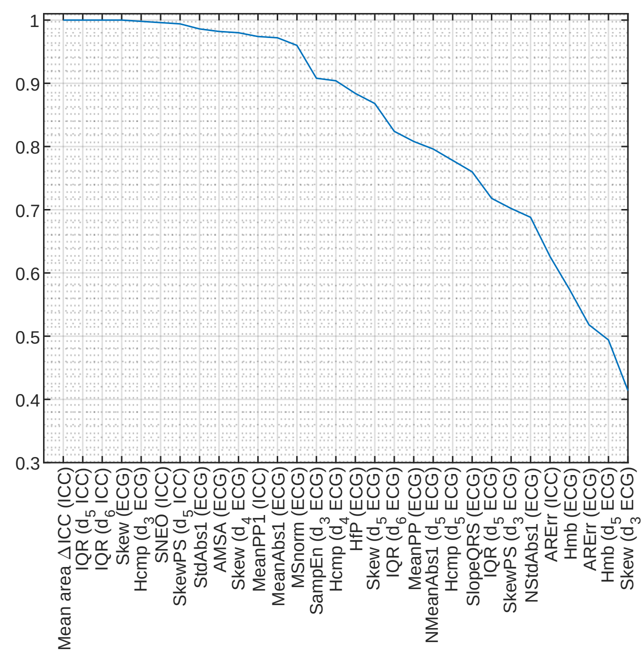

Fig. 6. Probability of selection for each feature when $N_f = 30$ and three classes were considered (TPEA/PPEA/PR)

TABLE II
PERFORMANCE METRICS REPRESENTED AS MEDIAN (IQR) FOR THE THREE-CLASS CLASSIFICATION PROBLEM

Signals	N_f	$\mathrm{Se}_{\mathrm{TPEA}}$	$\mathrm{Se}_{\mathrm{PPEA}}$	$\mathrm{Se}_{\mathrm{PR}}$	UMS	$\mathrm{F}_{1,\mathrm{TPEA}}$	$\mathrm{F}_{1,\mathrm{PPEA}}$	$\mathrm{F}_{1,\mathrm{PR}}$	$\mathrm{F}_{1\mathrm{m}}$
ECG, TI, CO_2	10*	70.3 (4.8)	50.4 (5.5)	78.4 (2.9)	66.2 (2.8)	67.9 (4.0)	41.1 (4.4)	69.0 (2.7)	59.2 (2.4)
ECG, TI, CO_2	20*	73.1 (3.7)	50.9 (4.6)	81.2 (2.4)	68.6 (2.4)	69.3 (2.4)	43.3 (3.3)	70.7 (2.5)	61.2 (1.8)
ECG, TI, CO_2	30*	74.4 (3.6)	50.2 (4.2)	82.3 (1.9)	68.8 (2.1)	69.3 (2.9)	44.3 (2.9)	71.1 (2.0)	61.5 (1.6)
ECG, TI, CO_2	40*	74.9 (3.7)	49.6 (3.7)	83.2 (1.5)	69.0 (2.1)	69.7 (2.8)	45.1 (3.0)	70.7 (1.7)	61.7 (1.5)
ECG	30	57.5 (4.5)	37.2 (5.5)	80.9 (2.7)	58.6 (2.6)	57.1 (2.8)	35.7 (4.4)	68.9 (1.9)	53.8 (2.2)
ECG, TI	30	71.8 (3.4)	47.7 (5.6)	81.5 (2.1)	66.9 (2.6)	65.8 (2.5)	42.9 (4.1)	70.8 (2.3)	59.8 (2.1)

* The final model included $N_f + 1$ features ($\mathrm{MEtCO_2}$)

PPEA. The ECG only and ECG+TI models presented a UMS of 58.6% and 66.9%, 25 and 33 points above that of a random guess.

Another key variable when identifying the circulation state is the duration of the signal segment. Chest compression therapy must be interrupted for the analysis to avoid artefacts in the ECG and TI. But these interruptions compromise blood flow in deteriorated circulation states and may negatively affect patient survival [41]. Consequently, the shorter the analysis segment the better. Fig. 7 shows the median (IQR) of per class F_1 scores of a $N_f = 30$ feature model as the duration of the analysis segment is shortened. From 1-s to 5-s windows F_1 increased only one point for PR, but almost 5 points for TPEA and PPEA. Increasing the analysis window was beneficial to discriminate the most challenging class, PPEA.

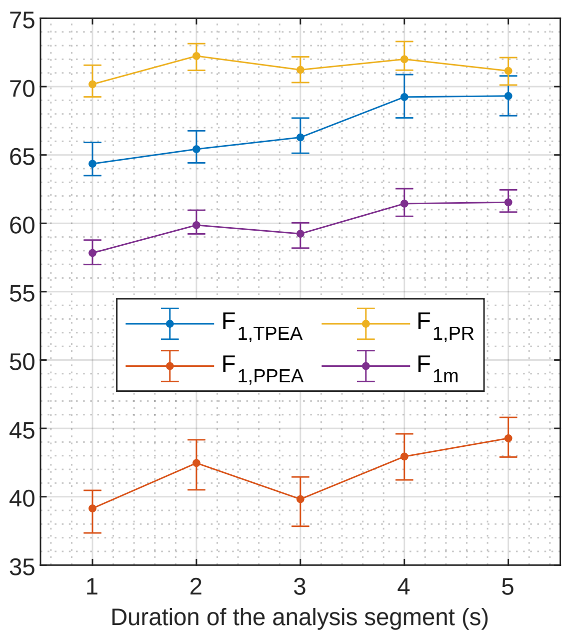

Fig. 7. Median (IQR) of per class F_1 in terms of the duration of the analysis segment.

B. Binary classification of circulation states

Binary classification of circulation states (PEA/PR or pulse/no-pulse classification) is a well known field of study in biosignal analysis applied to cardiac arrest [8], [9], [14]. Our model for this problem was constructed joining the TPEA

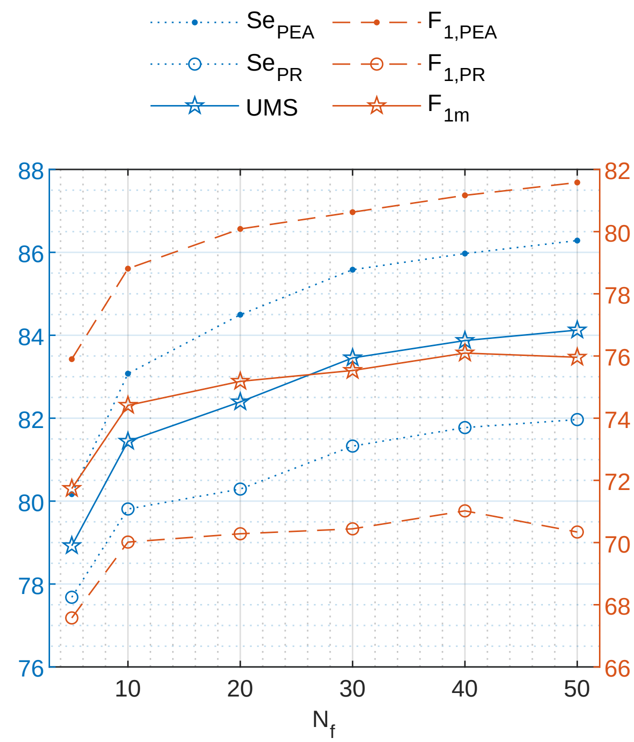

Fig. 8. Performance (%) of the prediction model in terms of the number of features included (N_f) for the two-class classification problem

and PPEA classes. The performance metrics as a function of the number of features in the RF model are shown in Fig. 8. The accuracy of the model increased substantially when going from a 5-feature to a 50-feature model, with an increase of 5 points in UMS. As reference, the performance of our model was compared in our dataset to those of the reference studies in binary circulation state classification [8], [9], [13], [19]. The results are shown in Table III. Moreover, since these methods ranged from ECG only to multimodal methods including ECG, TI and CO_2 the analysis was further stratified to include models with features from the different signals. Our model outperformed the state of the art PEA/PR classification models. The UMS/$\mathrm{F}_{1\mathrm{m}}$ of our models were 5/6 and 4/3 points larger than the next best methods based on ECG+TI and ECG+TI+CO_2, respectively. In all cases the AUC of our models was 1 to 4 points larger.

Fig. 9 shows the average feature ranking for all training partitions for a model with 30 features. It can be observed

TABLE III
PERFORMANCE METRICS REPRESENTED AS MEDIAN (INTERQUARTILE RANGE) FOR THE TWO-CLASS CLASSIFICATION PROBLEM

	Signals	N_f	$\mathrm{Se_{PEA}}$	$\mathrm{Se_{PR}}$	UMS	$\mathrm{F_{1,PEA}}$	$\mathrm{F_{1,PR}}$	$\mathrm{F_{1m}}$	AUC
Risdal et al. [8]	ECG, TI	17	78.8 (2.7)	78.0 (3.1)	78.3 (2.2)	74.0 (1.8)	64.9 (2.0)	69.4 (1.7)	0.84 (0.02)
Risdal et al. [8]	ECG, TI	12	80.1 (3.2)	77.6 (2.2)	78.6 (2.2)	74.6 (2.3)	65.1 (2.0)	69.7 (1.8)	0.84 (0.02)
Alonso et al. [9]	ECG, TI	6	68.8 (1.7)	77.3 (1.4)	73.1 (1.4)	67.7 (1.3)	65.7 (1.9)	66.7 (1.4)	0.84 (0.02)
Elola et al. [13]	ECG	9	77.9 (2.2)	80.2 (2.6)	78.9 (1.6)	74.6 (1.2)	67.9 (1.8)	71.2 (1.5)	0.84 (0.01)
Elola et al. [19]	ECG, TI, CO_2	10	79.9 (2.2)	81.1 (2.2)	80.4 (1.9)	77.0 (2.0)	79.4 (2.0)	73.0 (1.7)	0.87 (0.01)
This study	ECG, TI, CO_2	10*	83.1 (3.0)	79.8 (2.8)	81.5 (1.8)	78.8 (2.5)	70.0 (2.9)	74.5 (1.9)	0.87 (0.02)
This study	ECG, TI, CO_2	20*	84.5 (2.5)	80.3 (2.3)	82.4 (1.7)	80.1 (1.7)	70.3 (2.5)	75.3 (1.5)	0.88 (0.01)
This study	ECG, TI, CO_2	30*	85.6 (2.4)	81.3 (2.0)	83.2 (1.9)	80.6 (1.7)	70.4 (2.5)	75.6 (1.8)	0.89 (0.01)
This study	ECG, TI, CO_2	40*	86.0 (2.1)	81.8 (2.1)	83.9 (1.7)	81.2 (1.7)	71.0 (2.6)	76.2 (1.8)	0.89 (0.01)
This study	ECG	30	76.4 (2.6)	80.4 (4.0)	78.4 (2.2)	74.4 (1.8)	68.5 (2.1)	71.4 (1.6)	0.85 (0.01)
This study	ECG, TI	30	85.9 (2.2)	80.5 (2.3)	83.1 (1.8)	80.6 (1.5)	70.3 (2.7)	75.5 (1.8)	0.88 (0.01)

* The final model included $N_f + 1$ features ($\mathrm{MEtCO_2}$)

that the model includes 7 ICC features, 3 of which have the highest probability. Some of the most important features were first proposed in this study for PEA/PR classification.

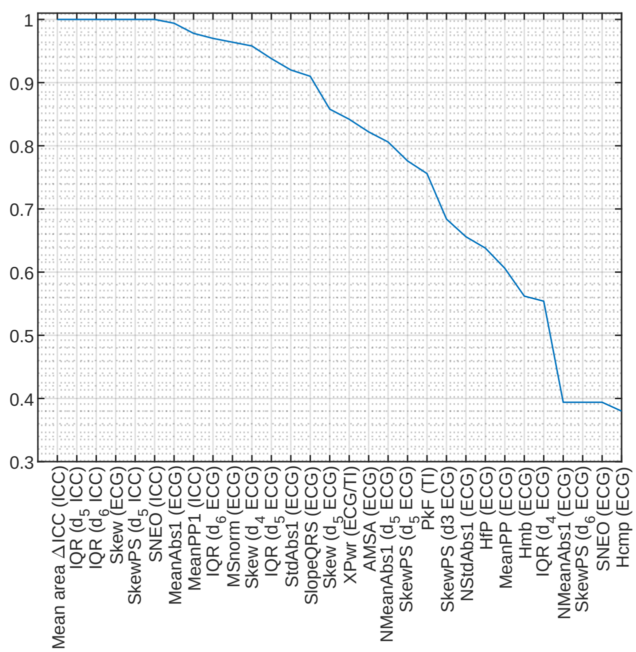

Fig. 9. Probability of selection for each feature when $N_f = 30$ and two classes were considered (PEA/PR)

VI. DISCUSSION

This study is, to the best of our knowledge, the first to address detailed circulation state classification models during OHCA. One of the key difficulties when assessing the circulation state during OHCA is the lack of a reliable source of information for the ground truth annotations. We were able to circumvent this difficulty by using a rich experimental biomedical signal dataset of 210 OHCA cases, in which patients were cannulated and the IBP signal was recorded in a prehospital setting. Then, the models to determine the circulation state were developed using signals routinely acquired during OHCA treatment like the ECG, TI or the capnogram. Moreover, different models were designed for ECG only, ECG+TI and ECG+TI+CO_2 situations, to address the differences in availability of biomedical signals in current defibrillator models used to treat OHCA.

Our best model to classify circulation states had a median $\mathrm{F_{1m}}$ and UMS of 61.5% and 68.8%, i.e. 35-points above a random guess for a 3-class problem. The model used ECG, TI and CO_2 features, in fact $\mathrm{MEtCO_2}$ was important to differentiate TPEA and PPEA. For a 30 feature model removing the $\mathrm{MEtCO_2}$ lowered the TPEA and PPEA sensitivities from 74.4% to 71.8%, and from 50.2% to 47.7%, respectively. The $\mathrm{MEtCO_2}$ values were significantly larger in PPEA than in TPEA, with median values of 32.1 (25.2-42.8) mmHg and 9.2 (5.0-24.1) mmHg, respectively. These conclusions are coherent with those observed in previous studies [19], [24]. In fact, $\mathrm{EtCO_2}$ showed positive correlations with blood pressure measurements [42], which may explain its value to differentiate circulation states during PEA.

In this study we introduced a novel feature extraction method from the ECG and TI combining multiresolution waveform analysis based on the SWT and a Kalman smoother to obtain the ICC. When our methods were compared to those proposed in the literature for the binary classification of circulation states (PEA/PR) [8], [9], [13], [19], our models outperformed all previous models (see Table III). This proves the value of the feature extraction methods introduced in this study, in particular the value of the Kalman smoother to obtain the ICC. When compared to a previous approach to obtain the ICC based on the RLS method [9] and following the same procedure, our Kalman smoother improved the median UMS by 4.5 and 2 points for the detailed and the binary classification of circulation states, respectively.

The detailed automatic classification of circulation states of OHCA patients may contribute to improve treatment, particularly, in guiding the administration of vasoconstrictors like epinephrine. Currently, the European Resuscitation Council and the American Heart Association recommend different treatments for pseudo and true PEA [4], [43]. The distinction between PEA states, and the identification of spontaneous circulation, are currently done by expert clinicians in stressful treatment conditions, it is not very accurate, and involves long interruptions in therapy [44]–[46]. Integrating the algorithms introduced in this study in current monitor defibrillators would contribute to a better identification of circulation states, and could serve experts as a clinical decision support tool during OHCA treatment.

The proposed algorithms provided Se values of 86% and 81.8% for PEA and PR, respectively. However, for clinical practice minimum accuracy figures would be required. For instance, the American Heart Association recommends sensitivities above 90% and 95% for the automatic shock/no-shock decision algorithms before being used in automated external defibrillators [47]. No such recommendations exist for pulse detection algorithms, but our algorithms, despite outperforming state of the art solutions, are still far from the accuracies needed in clinical practice. However, if the algorithms were to be used as a diagnosis support tool by the rescuer in combination with other information provided by the defibrillator, the accuracy requirements could be relaxed and the solution integrated in every day practice.

The precision of the classification algorithms could benefit from further research. Including a larger dataset to develop the models, or using advanced machine learning techniques could enhance the performance of the classifiers. Obtaining a larger patient cohort is a difficult task, as IBP is rarely acquired in OHCA. However, unlabeled data could be used to augment the datasets using techniques like semi-supervised learning [48], as the ECG, TI and the capnogram are routinely acquired signals. Deep learning algorithms have already been proven to outperform binary classifiers of circulation states [14], and other signals such as the PPG have shown promising results [18]. Future solutions might benefit from additional signals in the classification model and more sophisticated machine learning architectures.

VII. Conclusions

This study introduces multimodal biosignal processing and machine learning algorithms for the classification of circulation states during OHCA, and it is the first time that the automatic detection of detailed circulation states is addressed. These algorithms could serve as an important clinical decision tool for clinicians for the adequate administration of medication during OHCA treatment, and in decisions such as transport to hospital for post-resuscitation care.

Acknowledgment

Authors are gratefull to collaborators Fred.W. Chapman and Fredrick Arnwald for their support and valuable contributions to this study.

References

[1] J.-T. Gräsner *et al.*, "EuReCa ONE: 27 Nations, ONE Europe, ONE Registry: A prospective one month analysis of out-of-hospital cardiac arrest outcomes in 27 countries in europe," *Resuscitation*, vol. 105, pp. 188–195, 2016.

[2] E. J. Benjamin *et al.*, "Heart disease and stroke statistics-2018 update: a report from the american heart association." *Circulation*, vol. 137, no. 12, p. e67, 2018.

[3] G. D. Perkins *et al.*, "European resuscitation council guidelines for resuscitation 2015: Section 2. adult basic life support and automated external defibrillation," *Resuscitation*, vol. 95, pp. 81–99, 2015.

[4] J. Soar *et al.*, "Section 3. adult advanced life support: European resuscitation council guidelines for resuscitation 2015." *Resuscitation*, 2015.

[5] E. Skogvoll *et al.*, "Dynamics and state transitions during resuscitation in out-of-hospital cardiac arrest," *Resuscitation*, vol. 78, no. 1, pp. 30–37, 2008.

[6] J. Berdowski *et al.*, "Chest compressions cause recurrence of ventricular fibrillation after the first successful conversion by defibrillation in out-of-hospital cardiac arrest," *Circulation: Arrhythmia and Electrophysiology*, vol. 3, no. 1, pp. 72–78, 2010.

[7] J. P. Nolan *et al.*, "European resuscitation council and european society of intensive care medicine guidelines for post-resuscitation care 2015: section 5 of the european resuscitation council guidelines for resuscitation 2015," *Resuscitation*, vol. 95, pp. 202–222, 2015.

[8] M. Risdal *et al.*, "Automatic identification of return of spontaneous circulation during cardiopulmonary resuscitation," *IEEE Transactions on Biomedical Engineering*, vol. 55, no. 1, pp. 60–68, 2008.

[9] E. Alonso *et al.*, "Circulation detection using the electrocardiogram and the thoracic impedance acquired by defibrillation pads," *Resuscitation*, vol. 99, pp. 56–62, 2016.

[10] B. Eberle *et al.*, "Checking the carotid pulse check: diagnostic accuracy of first responders in patients with and without a pulse," *Resuscitation*, vol. 33, no. 2, pp. 107–116, 1996.

[11] J. Tibballs and P. Russell, "Reliability of pulse palpation by healthcare personnel to diagnose paediatric cardiac arrest," *Resuscitation*, vol. 80, no. 1, pp. 61–64, 2009.

[12] M. Ruppert *et al.*, "Checking for breathing: evaluation of the diagnostic capability of emergency medical services personnel, physicians, medical students, and medical laypersons," *Annals of emergency medicine*, vol. 34, no. 6, pp. 720–729, 1999.

[13] A. Elola *et al.*, "ECG-based pulse detection during cardiac arrest using random forest classifier," *Medical & Biological Engineering & Computing*, vol. 57, no. 2, pp. 453–462, Feb. 2019.

[14] A. Elola *et al.*, "Deep Neural Networks for ECG-Based Pulse Detection during Out-of-Hospital Cardiac Arrest," *Entropy*, vol. 21, no. 3, p. 305, Mar. 2019.

[15] N. A. Cromie *et al.*, "The impedance cardiogram recorded through two electrocardiogram/defibrillator pads as a determinant of cardiac arrest during experimental studies*," *Critical Care Medicine*, vol. 36, no. 5, p. 1578, May 2008.

[16] A. Elola *et al.*, "Convolutional Recurrent Neural Networks to Characterize the Circulation Component in the Thoracic Impedance during Out-of-Hospital Cardiac Arrest," in *2019 41st Annual International Conference of the IEEE Engineering in Medicine and Biology Society (EMBC)*, Jul. 2019, pp. 1921–1925.

[17] J. M. Ruiz *et al.*, "Circulation assessment by automated external defibrillators during cardiopulmonary resuscitation," *Resuscitation*, vol. 128, pp. 158–163, 2018.

[18] R. W. Wijshoff *et al.*, "Photoplethysmography-based algorithm for detection of cardiogenic output during cardiopulmonary resuscitation," *IEEE Transactions on Biomedical Engineering*, vol. 62, no. 3, pp. 909–921, 2014.

[19] A. Elola *et al.*, "Capnography: A support tool for the detection of return of spontaneous circulation in out-of-hospital cardiac arrest," *Resuscitation*, vol. 142, pp. 153–161, Sep. 2019.

[20] T. Aufderheide *et al.*, "Etiology, electrophysiology, and myocardial mechanics of pulseless electrical activity," *Cardiac arrest: the science and practice of resuscitation medicine*, vol. 22, p. 426, 2007.

[21] N. A. Paradis *et al.*, "Aortic pressure during human cardiac arrest: identification of pseudo-electromechanical dissociation," *Chest*, vol. 101, no. 1, pp. 123–128, 1992.

[22] R. J. Myerburg *et al.*, "Pulseless electric activity: definition, causes, mechanisms, management, and research priorities for the next decade: report from a national heart, lung, and blood institute workshop," *Circulation*, vol. 128, no. 23, pp. 2532–2541, 2013.

[23] U. A. P. Flato *et al.*, "Echocardiography for prognostication during the resuscitation of intensive care unit patients with non-shockable rhythm cardiac arrest," *Resuscitation*, vol. 92, pp. 1–6, 2015.

[24] G. Prosen *et al.*, "Impact of modified treatment in echocardiographically confirmed pseudo-pulseless electrical activity in out-of-hospital cardiac arrest patients with constant end-tidal carbon dioxide pressure during compression pauses," *Journal of International Medical Research*, vol. 38, no. 4, pp. 1458–1467, 2010.

[25] M. Y. C. Chia *et al.*, "Comparison of outcomes and characteristics of emergency medical services (ems)-witnessed, bystander-witnessed, and unwitnessed out-of-hospital cardiac arrests in singapore," *Prehospital Emergency Care*, vol. 23, no. 6, pp. 847–854, 2019.

[26] C. Weiser *et al.*, "Initial electrical frequency predicts survival and neurological outcome in out of hospital cardiac arrest patients with pulseless electrical activity," *Resuscitation*, vol. 125, pp. 34–38, 2018.

[27] L. Littmann *et al.*, "A simplified and structured teaching tool for the evaluation and management of pulseless electrical activity," *Medical Principles and Practice*, vol. 23, no. 1, pp. 1–6, 2014.

[28] D. Bergum *et al.*, "Ecg patterns in early pulseless electrical activity-associations with aetiology and survival of in-hospital cardiac arrest," *Resuscitation*, vol. 104, pp. 34–39, 2016.

[29] D. L. Donoho and J. M. Johnstone, "Ideal spatial adaptation by wavelet shrinkage," *biometrika*, vol. 81, no. 3, pp. 425–455, 1994.

[30] I. Daubechies, *Ten lectures on wavelets*. Siam, 1992, vol. 61.

[31] H. Losert *et al.*, "Thoracic-impedance changes measured via defibrillator pads can monitor signs of circulation," *Resuscitation*, vol. 73, no. 2, pp. 221–228, 2007.

[32] J. Ruiz *et al.*, "Reliable extraction of the circulation component in the thoracic impedance measured by defibrillation pads," *Resuscitation*, vol. 84, no. 10, pp. 1345–1352, 2013.

[33] Z. Zhao *et al.*, "Spectro-temporal ecg analysis for atrial fibrillation detection," in *2018 IEEE 28th International Workshop on Machine Learning for Signal Processing (MLSP)*. IEEE, 2018, pp. 1–6.

[34] S. Haykin, *Kalman filtering and neural networks*. John Wiley & Sons, 2004, vol. 47, ch. 1.

[35] P. S. Hamilton and W. J. Tompkins, "Quantitative investigation of qrs detection rules using the mit/bih arrhythmia database," *IEEE transactions on biomedical engineering*, no. 12, pp. 1157–1165, 1986.

[36] E. Aramendi *et al.*, "Feasibility of the capnogram to monitor ventilation rate during cardiopulmonary resuscitation," *Resuscitation*, vol. 110, pp. 162–168, 2017.

[37] I. Isasi *et al.*, "A machine learning shock decision algorithm for use during piston-driven chest compressions," *IEEE Transactions on Biomedical Engineering*, vol. 66, no. 6, pp. 1752–1760, 2018.

[38] I. Isasi *et al.*, "Automatic cardiac rhythm classification with concurrent manual chest compressions," *IEEE Access*, vol. 7, pp. 115 147–115 159, 2019.

[39] A. B. Rad *et al.*, "Ecg-based classification of resuscitation cardiac rhythms for retrospective data analysis," *IEEE Transactions on Biomedical Engineering*, vol. 64, no. 10, pp. 2411–2418, 2017.

[40] B. Chicote *et al.*, "Nonlinear energy operators for defibrillation shock outcome prediction," in *2016 Computing in Cardiology Conference (CinC)*. IEEE, 2016, pp. 61–64.

[41] C. Vaillancourt *et al.*, "The impact of increased chest compression fraction on return of spontaneous circulation for out-of-hospital cardiac arrest patients not in ventricular fibrillation," *Resuscitation*, vol. 82, no. 12, pp. 1501–1507, 2011.

[42] C. P. Kheng and N. H. Rahman, "The use of end-tidal carbon dioxide monitoring in patients with hypotension in the emergency department," *International journal of emergency medicine*, vol. 5, no. 1, p. 31, 2012.

[43] M. S. Link *et al.*, "Part 7: adult advanced cardiovascular life support: 2015 american heart association guidelines update for cardiopulmonary resuscitation and emergency cardiovascular care," *Circulation*, vol. 132, no. 18_suppl_2, pp. S444–S464, 2015.

[44] F. Lapostolle *et al.*, "Basic cardiac life support providers checking the carotid pulse: performance, degree of conviction, and influencing factors," *Academic emergency medicine*, vol. 11, no. 8, pp. 878–880, 2004.

[45] E. J. Clattenburg *et al.*, "Point-of-care ultrasound use in patients with cardiac arrest is associated prolonged cardiopulmonary resuscitation pauses: a prospective cohort study," *Resuscitation*, vol. 122, pp. 65–68, 2018.

[46] M. A. H. in't Veld *et al.*, "Ultrasound use during cardiopulmonary resuscitation is associated with delays in chest compressions," *Resuscitation*, vol. 119, pp. 95–98, 2017.

[47] R. E. Kerber *et al.*, "Automatic external defibrillators for public access defibrillation: recommendations for specifying and reporting arrhythmia analysis algorithm performance, incorporating new waveforms, and enhancing safety: a statement for health professionals from the american heart association task force on automatic external defibrillation, subcommittee on aed safety and efficacy," *Circulation*, vol. 95, no. 6, pp. 1677–1682, 1997.

[48] X. Zhaia *et al.*, "Semi-supervised learning for ecg classification without patient-specific labeled data," *Expert Systems with Applications*, p. 113411, 2020.